Inorganica Chimica Acta 362 (2009) 3987–3992

Contents lists available at ScienceDirect

Inorganica Chimica Acta

journal homepage: www.elsevier.com/locate/ica

Self-assembly of 2D zinc metal–organic frameworks based on mixed organic ligands

Fangna Dai, Haiyan He, Dongliang Gao, Fei Ye, Daofeng Sun *, Zhijian Pang, Lei Zhang, Guilin Dong, Changqiao Zhang *

Key Lab of Colloid and Interface Chemistry, Ministry of Education, School of Chemistry and Chemical Engineering, Shandong University, Jinan 250100, PR China

ARTICLE INFO

Article history:
Received 16 February 2009
Received in revised form 11 May 2009
Accepted 15 May 2009
Available online 23 May 2009

Keywords:
2D
Zinc
Metal–organic framework
Photoluminescence
Mixed organic ligands

ABSTRACT

Self-assembly of $Zn(NO_3)_2{\cdot}6H_2O$, 5-amino-2,4,6-triiodoisophthalic acid (H_2atiip) and 4,4′-bipyridine (bpy) or 1,3-di(4-pyridyl)propane (dpp) gave rise to three unusual zinc metal–organic frameworks, $Zn_2(bpy)_2(atiip)_2{\cdot}3H_2O{\cdot}2dmf$ (**1**), $Zn_8(dpp)_8(atiip)_8{\cdot}4H_2O$ (**2**), $Zn(dpp)(atiip){\cdot}(dmf){\cdot}(H_2O)$ (**3**). All complexes possess 2D layer frameworks constructed from 1D Zn-carboxylate tubular unit for **1**, 1D Zn-carboxylate helical chain for **2** and **3**. In **1** and **2**, the bpy or dpp act as both bridging and blocking ligands and the blocking ligands play an important role in the formation of the 2D layer frameworks. Both **2** and **3** contain two different large metallomacrocycles. Photoluminescence measurements of **1**–**3** in the solid state at room temperature show that all complexes exhibit luminescence, which can be assigned to an intraligand $\pi \rightarrow \pi^*$ transition or ligand-to-metal charge transfer (LMCT).

1. Introduction

Supramolecular chemistry and crystal engineering of metal–organic frameworks (MOFs) have received much attention of chemists due to its powerful function in design and synthesis of functional materials with interesting structures and desired topologies [1–5]. Carboxylate ligands as versatile organic linker have been widely used in the construction of MOFs with 1D, 2D, and 3D frameworks [6,7]. By introducing secondary organic ligands in the carboxylate systems, many metal–organic frameworks based on mixed organic ligands have been designed and synthesised [8,9]. In this regard, two types of pyridine-derivatives have been introduced in the carboxylate system as the secondary organic ligands based on the difference of their linking modes. 2,2′-bipyridine and its derivatives have been used as blocking ligand in the construction of low-dimensional frameworks due to their chelating coordination mode [10,11], and 4,4′-bipyridine and its derivatives usually adopt bridging coordination mode to connect two metal ions or clusters to give rise to high-dimensional frameworks [12,13], although a few examples with 4,4′-bipyridine as monodentate ligand have been explored [14,15].

On the other hand, the introduction of the bridging pyridine-based ligands into the carboxylate system can generate more topological structures than the single carboxylate system, despite the fact that it adds more difficulty in the prediction and control of the components or the structure of the product in the mixed ligands system due to the competition between the ligands. Our research focuses on the construction of MOFs based on mixed organic ligands and understanding the different roles of the mixed ligands in the formation of the framework. We select 5-amino-2,4,6-triiodoisophthalic acid (H_2atiip) as the assembly organic ligand considering its following characteristics: (i) it has two carboxylate groups, which can bridge metal ions in multiply coordination modes, similar to 1,3-bdc; (ii) the steric hindrance between the iodine atoms and the carboxyate groups provide the central benzene ring and the carboxylate groups the ability to not locate in a plane, which result in the face that the carboxylate groups connect to metal ion in different directions; (iii) the two carboxylate groups locate in the meta positions of the benzene ring and are not in a plane with the benzene ring, which may connect the metal ion to form tubular or helical structure. Very recently, by introducing 4,4-bipyridine in the carboxylate system, we synthesised a novel 1D zinc metal–organic nanotube exhibiting reversible adsorption of $(H_2O)_{12}$ cluster [16]. In this full paper, we report the synthesis, crystal structures and photoluminescence properties of three 2D zinc metal–organic frameworks, $Zn_2(bpy)_2(atiip)_2{\cdot}3H_2O{\cdot}2dmf$ (**1**), $Zn_8(dpp)_8(atiip)_8{\cdot}4H_2O$ (**2**), $Zn(dpp)(atiip){\cdot}(dmf){\cdot}(H_2O)$ (**3**), constructed from mixed organic ligands of H_2atiip and bpy or dpp.

2. Experimental

2.1. Materials and physical measurements

All chemicals used are as purchased without purification. H_2atiip, 4,4-bipy and 1,3-di(4-pyridyl)propane are bought from Alfa

* Corresponding authors. Tel./fax: +86 531 88364218.
E-mail addresses: dfsun@sdu.edu.cn (D. Sun), zhangchqiao@sdu.edu.cn (C. Zhang).

0020-1693/$ - see front matter Crown Copyright © 2009 Published by Elsevier B.V. All rights reserved.
doi:10.1016/j.ica.2009.05.038

Asian. Thermogravimetric experiments were performed using a TGA/SDTA851 instrument (heating rate of 10 °C/min, nitrogen stream). Elemental analyses (C, H, N) were obtained on a Perkin–Elmer 240 elemental analyzer. Photoluminescence spectra were performed on a Perkin Elmer LS 50B luminescence spectrometer.

2.2. Preparation of complexes

2.2.1. $[Zn_2(bpy)_2(atiip)_2]\cdot 3H_2O\cdot 2dmf$ (**1**)

$Zn(NO_3)_2\cdot 6H_2O$ (0.01 g, 0.0277 mmol), H_2atiip (0.01 g, 0.0179 mmol) and 4,4-bipy (0.01 g, 0.064 mmol) were dissolved in 8 mL mixed solvents of DMF, EtOH and H_2O (v/v = 5:2:1) in a 25 mL beaker. After being stirred at room temperature for ten minutes, the reaction mixture was filtered. The filtrate was left to stand at room temperature and the yellow crystals of 1 were obtained after one week (yield: 65%). Elemental *Anal.* Calc. for 1: C, 28.71; H, 2.29; N, 6.38%. Found: C, 28.55; H, 2.22; N, 6.09%.

2.2.2. $[Zn_8(dpp)_8(atiip)_8]\cdot 4H_2O$ (**2**)

$Zn(NO_3)_2\cdot 6H_2O$ (0.01 g, 0.0277 mmol), H_2atiip (0.10 g, 0.0179 mmol), 1,3-di(4-pyridyl)propane (0.01 g, 0.05 mmol) were dissolved in 10 mL mixed solvents of DMF, EtOH and H_2O (v/v = 5:2:1) in a 25 mL beaker. After being stirred at room temperature for 10 min, the beaker was left at 90 °C for 3 days. The resulting brown block crystals of **2** were collected in 75% yield on the basis of zinc. Elemental *Anal.* Calc. for 1: C, 35.57; H, 2.61; N, 6.03%. Found: C, 35.59; H, 2.51; N, 5.96%.

2.2.3. $[Zn(dpp)(atiip)]?(dmf)?(H_2O)$ (**3**)

$Zn(NO_3)_2\cdot 6H_2O$ (0.01 g, 0.0277 mmol), H_2atiip (0.10 g, 0.0179 mmol) and 1,3-di(4-pyridyl)propane (0.01 g, 0.05 mmol) were dissolved in 10 mL mixed solvents of DMF, EtOH and H_2O (v/v = 5:2:1) in a 25 mL beaker. After the mixture being stirred in the air for 10 min, the resulting yellow solution was allowed to evaporate at room temperature for 7 days to give block crystals of 3 in 50% yield. Elemental *Anal.* Calc. for 3: C, 31.62; H, 2.76; N, 6.15%. Found: C, 31.78; H, 2.52; N, 6.15%.

2.3. Crystal structures determinations

Crystallographic data for **1**–**3** were collected on a Bruker APEXII CCD diffractometer with Mo Kα (λ = 0.71073 Å) at room temperature. All structures were solved by the direct method using the SHELXS program of the SHELXTL package and refined by the full-matrix least-squares method with SHELXL [17,18]. The metal atoms in each complex were located from the E-maps, and other non-hydrogen atoms were located in successive difference Fourier syntheses and refined with anisotropic thermal parameters on F2. The hydrogen atoms were generated geometrically (C—H 0.96 Å). A summary of the crystallographic data are given in Table 1.

Table 1
Crystal data for complexes **1**–**3**.

Complex	1	2	3
Formula	$C_{36}H_{26}I_6N_6O_{11}Zn_2$	$C_{220}H_{192}I_{24}N_{32}O_{36}Zn_8$	$C_{24}H_{23}I_3N_4O_5Zn$
Formula weight	1610.77	7428.62	893.53
crystal size	0.2 × 0.1 × 0.05	0.3 × 0.2 × 0.1	0.15 × 0.1 × 0.1
crystal color	yellow	brown	yellow
crystal system	triclinic	monoclinic	monoclinic
space group	$P\bar{1}$	$P21/n$	$P21/n$
a (Å)	8.5532(8)	9.41530(10)	9.2478(5)
b (Å)	18.2032(18)	34.3442(5)	15.2758(9)
c (Å)	19.583(3)	18.6939(3)	20.3701(12)
α (°)	113.997(2)	90.00	90.00
β (°)	95.211(3)	99.8780(10)	91.7550(10)
γ (°)	99.150(2)	90.00	90.00
V (Å^3)	2708.8(5)	5955.26(14)	2876.3(3)
Z	2	1	4
D_{calc} (g cm^{-3})	1.975	2.071	2.063
F(0 0 0)	1500	3536	1696
μ (mm^{-1})	4.357	3.977	4.114
Goodness of fit	0.989	1.039	1.019
$R_1[I > 2\sigma(I)]$	0.0551	0.0404	0.0424
wR_2	0.1621	0.0947	0.0983

3. Results and discussion

3.1. Synthetic chemistry

Self-assembly process is an important method in construction of supramolecular architecture [19]. Many coordination complexes such as discrete molecules, 1D, 2D and 3D frameworks have been synthesised through supramolecular self-assembly. Complexes **1** and **3** were synthesised at room temperature, while complex **2** was obtained when heating the reaction mixture at 90 °C for 3 days, indicating the temperature has a significant influence on the formation of **2** and **3**. In complexes **1**–**3**, the zinc ions were first connected by the carboxylate ligand to generate a 1D tubular (for **1**) or helical (for **2** and **3**) subunit, which was further linked by the bridging bpy or dpp ligand to form the 2D layer frameworks. The bpy and dpp ligands act as both bridging and blocking ligand in **1** and **2**, respectively, while dpp ligand acts as only bridging ligand in **3**. Scheme 1 shows the coordination modes of the organic ligands in complexes **1**–**3**.

3.2. Crystal structure analysis

3.2.1. Crystal structure of complex (**1**)

As shown in Fig. 1, the asymmetric unit of **1** consists of two zinc ions, two atiip ligands, two and two halves of bpy ligands, and three uncoordinated water molecules. Zn1 is five-coordinated by three oxygen atoms from two atiip ligands, two nitrogen atoms from two bpy ligands, in a distorted trigonal bipyramidal geometry, while Zn2 is four-coordinated by three oxygen atoms from three atiip ligands, one nitrogen atom from bpy ligand in a tetrahedral geometry.

Two types of atiip ligands with different coordination modes are present in the structure: (a) one carboxylate group adopts bidentate chelating mode, chelating one Zn1 ion, whereas the other one adopts monodentate mode, coordinating to one Zn2 ion (scheme 1e); (b) one carboxylate group adopts bidentate bridging mode, linking one Zn1 and one Zn2 ions, the other one adopts monodentate coordination mode, connecting one Zn2 ion (scheme 1f). As expected, the carboxylate groups and the central benzene ring are not in a plane with the average dihedral angle of 88.3°. Thus, Zn1 and Zn2 are infinitely connected by atiip ligands to give rise to a 1D tubular unit (Fig. 2a and c), which can be considered as the basic building unit of **1**. To the best of our knowledge, only a

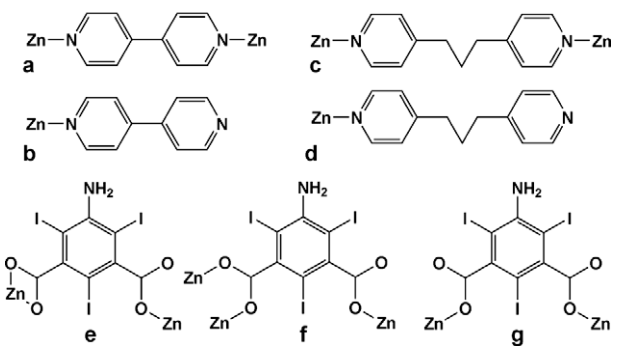

Scheme 1. The coordination modes of organic ligands in complexes **1**–**3**.

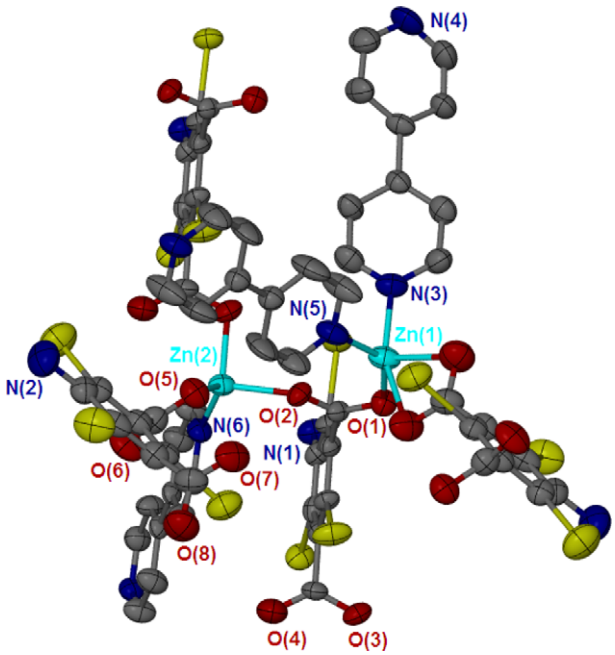

Fig. 1. The coordination environment of zinc ion in **1**.

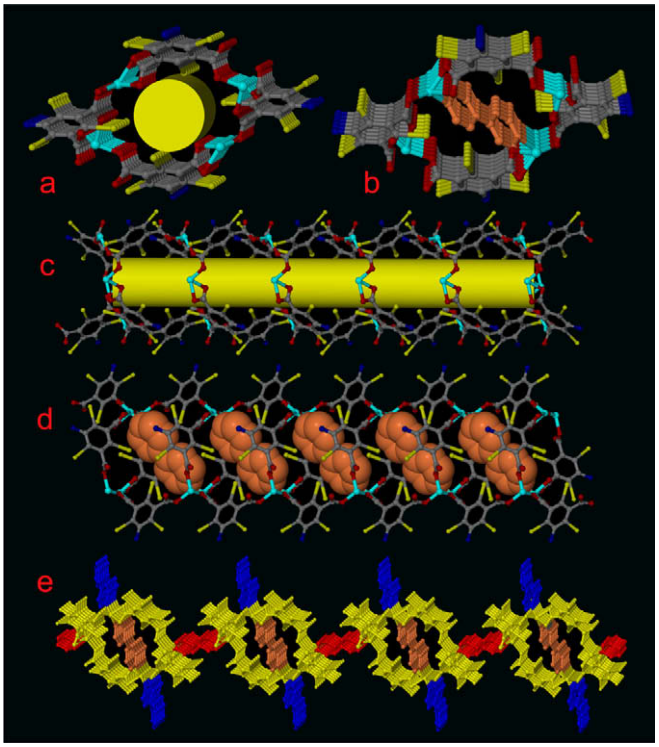

Fig. 2. (a) and (c) The 1D tubular unit generated by atiip ligands and zinc ions; (b) and (d) the 1D tubular unit showing bridging bpy ligands locate inside (brown color) to connect two Zn1 ions; (e) the final 2D layer generated by bpy connecting the 1D tubular units with two types of bpy in different colors, bridging bpy (brown, inside the tubular unit), bridging bpy (red, connecting the tubular units), blocking bpy (blue). (For interpretation of the references to color in this figure legend, the reader is referred to the web version of this article.)

few examples containing tubular unit have been reported in the literature [20–22].

The 1D tubular unit contains a 24-membered metallo-macrocycles made up of four atiip and four zinc ions with the dimensions of 9.6 × 5.5 Å (supporting information). It is interesting to note that there are two types of 4,4′-bipyridine molecules, which play different roles in the formation of **1**: one type of bpy ligand, which lies about independent inversion centers, acts as bridging ligand to connect two Zn ions (scheme 1a); while the other one, which locates in a general position, acts as blocking ligand (scheme 1b) to coordinate to one zinc ion to prevent complex **1** further extending. The bridging bpy ligand plays two roles in the formation of complex **1**: locating in the tubular unit to connect two Zn1 ions to further stabilize the tubular unit (Fig. 2b and d), and bridging two tubular units through coordinating to two Zn2 ions (Fig. 2e). Thus, the 1D tubular units are infinitely connected by bridging bpy ligand to generate a 2D layer structure, as shown in Fig. 2e. Hence, the atiip, bridging and blocking bpy connect zinc ions to form the 1D tubular unit, which is further connected by the bridging bpy to generate the final 2D layer framework. In the past reported MOFs containing 4,4′-bipy, the 4,4′-bipy acts as either bridging ligand to connect two metal ions or blocking ligand to coordinate to one metal ion, few examples that 4,4′-bipy acts as both bridging and blocking ligand have been documented in the literature [22–27].

All the blocking ligands of bpy point out of the layer. The π–π interactions (3.7 Å) between blocking bpy ligands in different layers as well as the strong N–I interactions (2.997 Å) further connect the 2D layers into a 3D porous supramolecular architecture, as shown in Fig. 3. The dimensions of the channels are 15.3 × 7.0 Å, in which uncoordinated water molecules reside. It should be pointed out that the N–I contact is very short in **1**. Normally, the N–X (X = F, Cl, Br, and I) contact falls into the range of 3.0–3.5 Å [28], and the examples such as in **1** that the N–I contact is less than 3.0 Å is quite rare.

3.2.2. Crystal structure of complex (*2*)

Complex **2** was synthesised in a solvothermal condition by use of 1,3-di(4-pyridyl)propane as the secondary organic ligand. The asymmetric unit of **2** consists of two zinc ions, two atiip ligands, three dpp ligands and one uncoordinated water molecule. As shown in Fig. 4, Zn1 is four-coordinated by two oxygen atoms from two atiip ligands, two nitrogen atoms from two dpp ligands, in a tetrahedral geometry. One of remaining carboxyl oxygen atoms has a weak coordination to Zn1 ion with the distance of 2.313 Å, thus the geometry of Zn1 ion can also be considered as a pseudo trigonal bipyramidal environment. Zn2 is four-coordinated by two oxygen atoms and two nitrogen atoms from different ligands in a tetrahedral geometry.

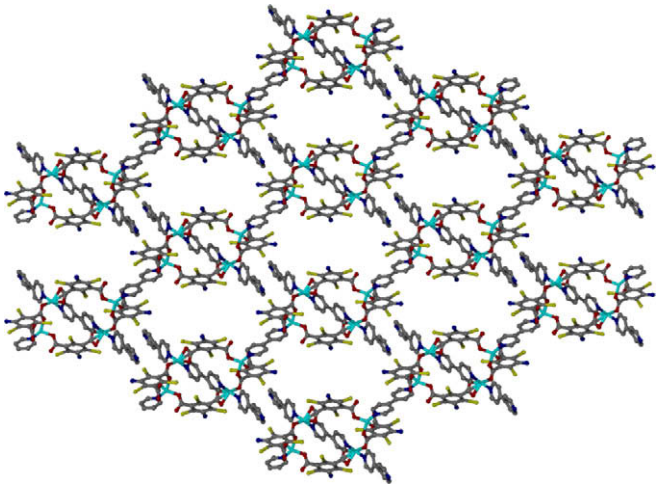

Fig. 3. The 3D porous supramolecular architecture of **1**.

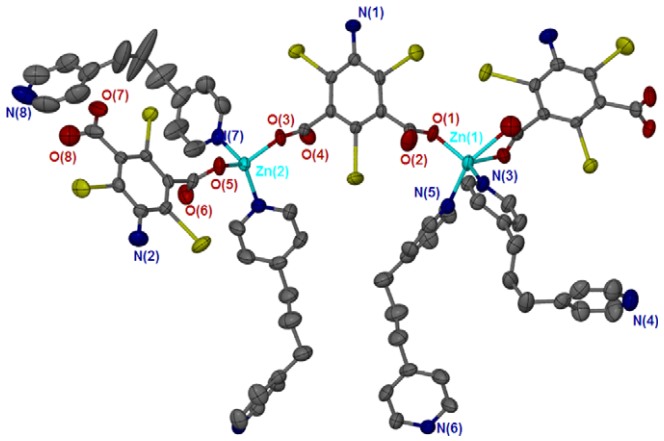

Fig. 4. The coordination environment of central zinc ions in **2**.

As found in complex **1**, there are two types of atiip ligands which possess different coordination modes in 2, as shown in scheme 1e and g. Thus, Zn1 and Zn2 ions are infinitely connected by atiip ligand to result in the formation of a left- or right-handed helical chain (Fig. 2a and b), in which the two types of atiip are alternant. The nearest Zn–Zn distance in the chain is 9.437 Å. The average dihedral angle between the carboxylate groups and the central benzene ring is 92.3°, which is slightly larger than that in **1**. The helical chains are further connected by the bridging dpp (scheme 1c) to generate a 2D layer structure with the separation of the helical chains of 13.369 Å. The remaining coordination sites of Zn1 and Zn2 ions are occupied by the blocking ligands of dpp (scheme 1d), which locate above or below the layer to prevent further extending into high dimensional framework. The left- and right-handed helical chains are equal in the layer, thus, the whole structure is achiral.

The layer can also be viewed as ladders sharing legs, in which the legs are formed by Zn-atiip helical chains and rungs by the bridging dpp ligands. It is interesting to note that the layer contains two different metallo-macrocycles: one is a 40-membered metallo-macrocycles (12.4 × 4.4 Å) made up of two atiip ligands, two bridging dpp ligands and four zinc ions; the other one is a 72-membered metallo-macrocycles (30.7 × 7.2 Å) made up of six atiip ligands, two bridging dpp and eight zinc ions, as shown in Fig. 5e and f, respectively. Hence, the 2D layer can also be considered as formed by infinitely sharing 40-membered and 72-membered metallo-macrocycles [28,29]. If Zn1 and Zn2 ions are treated as a single node, then complex **2** has a graphite-like (6,3) net, as shown in Fig. 5g.

3.2.3. Crystal structure of complex (*3*)

Single crystal X-ray diffraction reveals that complex **3** crystallizes in monoclinic space group *P*21/*n* and has a 2D layer framework possessing a (4,4) net. The asymmetric unit of **3** contains one zinc ion, one atiip ligand, one dpp ligand and one uncoordinated dmf molecule. As shown in Fig. 6, the central zinc ion is four-coordinated by two oxygen atoms from different atiip ligands and two nitrogen atoms from different dpp in a tetrahedral geometry with the average Zn–O and Zn–N distances of 1.943(4) and 2.034(5) Å, respectively.

Different from complexes **1** and **2**, both the carboxylate groups of atiip ligand in **3** adopt mono-dentate bridging mode to connect one zinc ion (scheme 1g). The average dihedral angle between the carboxylate groups and the central benzene ring is 94°, which is slight larger than that in **1** and **2**. Thus, the zinc ions are infinitely connected by atiip ligands to generate a 2_1 helical chain with the nearest Zn-Zn distance in the chain being 9.532 Å (Fig. 7a). The 2_1 helical chains are further connected by the bridging dpp ligands to give rise to a 2D layer structure with the nearest Zn–Zn distance between the helical chains of 11.543 Å (Fig. 7c and d). Since the 2_1 left- and right-handed helical chains are alternant and equal in the layer, thus, the whole structure is achiral.

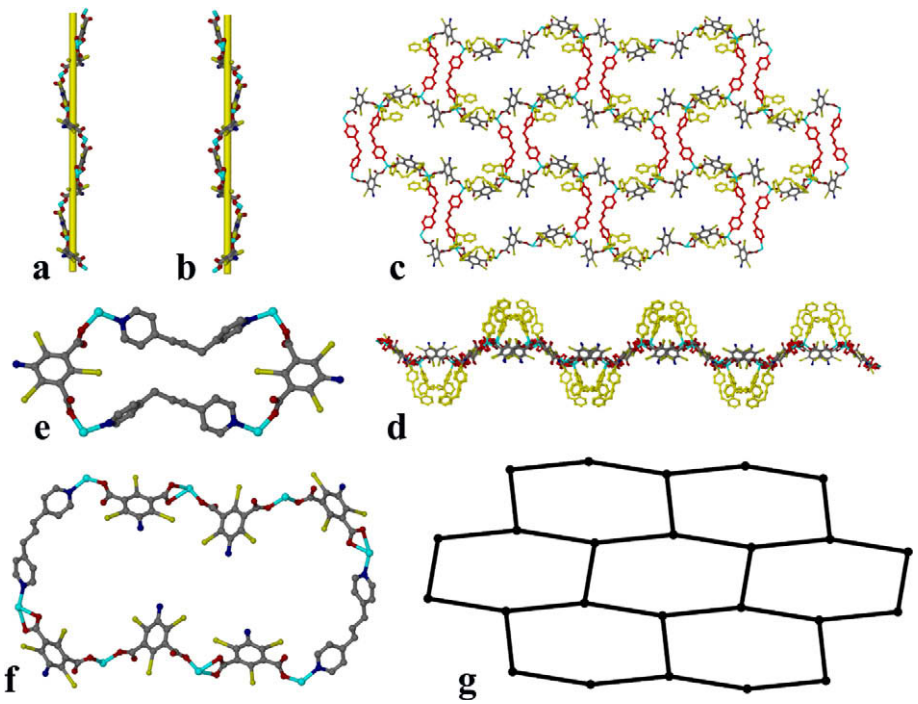

Fig. 5. (a) and (b) The left- and right-handed Zn-carboxylate helical chains; (c) and (d) the 2D layer containing large void with bridging dpp represented as red color and blocking dpp as yellow color; (e) the small 40-membered metallo-macrocycles; (f) the large 72-membered metallo-macrocycles; (g) the graphite-like (6,3) net representing the ligand and metal ions schematically. (For interpretation of the references to color in this figure legend, the reader is referred to the web version of this article.)

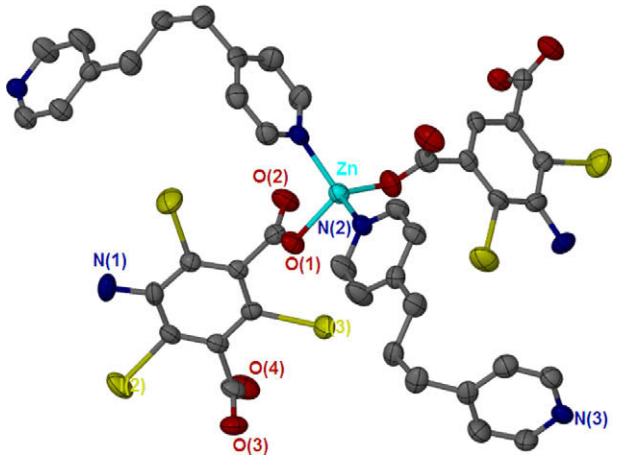

Fig. 6. The coordination environment of central zinc ion in **3**.

The layer can also be viewed as consisting of ladders sharing legs, in which the vertical bar are formed by Zn-atiip 2_1 helical chains and rungs by dpp ligands. As in **2**, the 2D layer contains two different metallo-macrocycles. Although both are 40-membered metallo-macrocycles made up of two atiip ligands, two dpp ligands and four zinc ions, there are slight difference due to the amino-group of atiip ligands pointing to different directions. One adopts head-to-head mode, in which the two atiip ligands locate inside the metallomacrocycles with the size of the metallomacrocycles being 15 × 4 Å (Fig. 7e); the other one adopts tail-to-tail mode, in which the two atiip ligands locate outside the metallomacrocycles with the size of the metallomacrocycles being 11.8 × 12.2 Å (Fig. 7f). If the atiip and dpp ligands can be considered as linear linkers and the zinc ion as single node, then complex **3** possesses a (4,4) net, as shown in Fig. 7g.

3.3. Thermal stabilities of complexes *1–3*

Thermogravimetric analysis showed that **1**, **2** and **3** have high thermal stabilities. For **1**, the gradual weight loss of 11.0% from 45 to 200 °C corresponds to the loss of three uncoordinated water molecules and two uncoordinated dmf molecules in the lattice (calc.: 11.4%). There is no further weight loss from 200 to 350 °C, and after that, **1** starts to decompose. For **2**, we did not find the loss of the uncoordinated water molecule. The first weight loss of 10.0% from 280 to 310 °C corresponds to the loss of one blocking dpp ligand (calc.: 10.7%). The second weight loss of 10.0% from 310 to 410 °C corresponds to the loss of the second blocking dpp ligand (calc.: 10.7%), and after 420 °C, **2** starts to decompose. For **3**, the gradual weight loss of 9.3% from 45 to 290 °C corresponds to the loss of one uncoordinated dmf and one uncoordinated water molecule in the lattice (calc.: 10.1%), and after 290 °C, **3** starts to decompose.

3.4. Photoluminescence properties of complexes *1–3*

On the basis of current research on luminescent MOFs, the emission of coordination polymers can be assigned to a ligand-to-metal charge transfer (LMCT) [30], metal-to-ligand charge transfer (MLCT) [31] or to an intraligand $\pi \rightarrow \pi^*$ transition. In general, metal coordination significantly influences fluorescence prop-

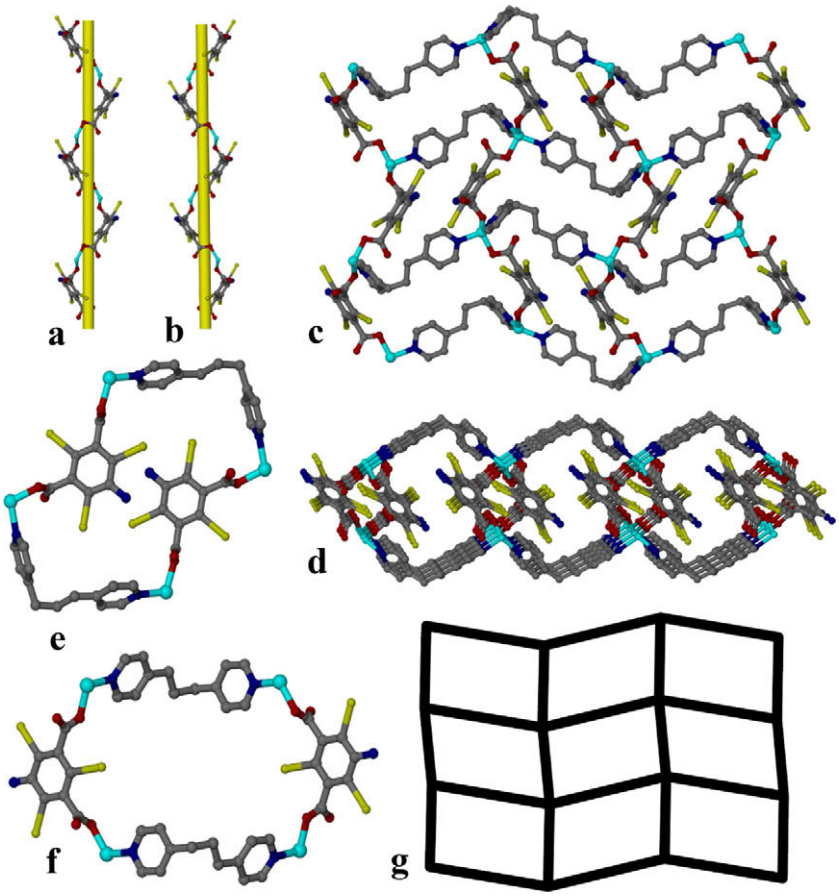

Fig. 7. (a) and (b) The left- and right-handed Zn-carboxylate helical chains; (c) and (d) the 2D layer; (e) the 40-membered metallo-macrocycles with the two amino-groups of the two atiip ligands adopting head-to-head arrangement; (f) the 40-membered metallo-macrocycles with the two amino-groups of the two atiip ligands adopting tail-to-tail arrangement; (g) the (4,4) net of **3**.

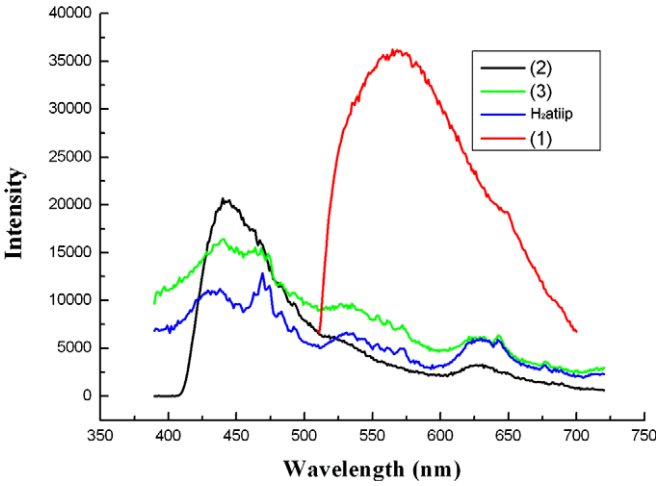

Fig. 8. Photoluminescence emission spectra for H_2atiip, **1**, **2** and **3** in the solid state at room temperature.

erties in MOFs (compared to organic ligands), an important property to consider when trying to synthesize new luminescent materials. The solid state fluorescence spectra of **1**, **2** and **3** have been measured and are depicted in Fig. 8. At room temperature, **1** shows moderated luminescence with emission maxima at 570 nm upon excitation at 420 nm in solid state (as powder samples). Complexes **2** and **3** exhibit similar luminescence at λ_{max} = 440 nm (upon excitation at 370 nm), although the intensity is slightly different. The emissions of **2** and **3** can probably be assigned to an intraligand $\pi \rightarrow \pi^*$ transition [32], as free H_2atiip ligand possesses similar emission in the solid state. These observations suggest that the coordination of the atiip ligand with Zn^{2+} ions has no influence on the emission mechanism of the metal–organic coordination polymers [33], although increasing the intensity of intraligand fluorescent emission due to the coordination of atiip ligand to the metal ion to increase the rigidity of the ligand and reduce the nonradiative decay of the intraligand excited state [34]. These emissions can be assigned to the ligand-to-metal charge transfer [30].

4. Conclusions

In summary, three 2D photoluminescent zinc metal–organic frameworks based on mixed organic ligands of carboxylate and 4,4′-bipy or 1,3-di(pyridin-4-yl)propane have been synthesised and characterized. Complexes **1** and **2** contain both blocking bpy or dpp and bridging bpy or dpp, which play different roles in the formation of the 2D layer frameworks: the bridging bpy or dpp ligands directly take part in the extension of the framework by bridging zinc ions, and the blocking bpy or dpp act as terminal ligand to prevent the 2D layer extending into 3D network. Both complexes **2** and **3** contain different large metallomacrocycles, which are quite rare in the literature. In all three complexes, due to the non-planarity of the carboxylate ligand, the zinc ions are first connected by the carboxylate ligand to generate a 1D tube or helical chain, which can be considered as the building unit of the whole structure. The 1D tubular or helical subunit is further connected by the bridging bpy or dpp to result in the formation of the 2D layer framework. All the blocking ligands in **1** and **2** adopt monodentate coordination mode and the remaining nitrogen atom of the ligand is available for coordinating to other metal ion. Thus, complexes **1** and **2** may act as the synthetic intermediate to assemble high-dimensional MOFs. Studies on this subject as well as constructing 3D porous metal–organic frameworks with these mixed organic ligands are currently underway.

Acknowledgments

This work was supported by the National Natural Science Foundation of China (Grant 20701025), the Natural Science Foundation of Shandong Province (Y2008B01), 973 Program (No. 2008CB617508), and Shandong University.

Appendix A. Supplementary data

CCDC 714724, 714723 and 714725 contain the supplementary crystallographic data for complexes **1**, **2** and **3**. These data can be obtained free of charge from The Cambridge Crystallographic Data Centre via www.ccdc.cam.ac.uk/data_request/cif.

Supplementary data associated with this article can be found, in the online version, at doi:10.1016/j.ica.2009.05.038.

References

[1] S.R. Batten, R. Robson, Angew. Chem., Int. Ed. 37 (1998) 1461.
[2] S. Kitagawa, R. Kitaura, S.-I. Noro, Angew. Chem., Int. Ed. 43 (2004) 2334.
[3] M. Eddaoudi, D.B. Moler, H. Li, B. Chen, T.M. Reineke, M. O'Keeffe, O.M. Yaghi, Acc. Chem. Res. 34 (2001) 319.
[4] O.R. Evans, W.B. Lin, Acc. Chem. Res. 35 (2002) 511.
[5] B. Moulton, M.J. Zaworotko, Chem. Rev. 101 (2001) 1629.
[6] L. Pan, M.B. Sander, X. Huang, J. Li, M.R. Smith Jr., E.W. Bittner, B.C. Bockrath, J.K. Johnson, J. Am. Chem. Soc. 126 (2004) 1308.
[7] S.S.Y. Chui, S.M.F. Lo, J.P.H. Charmant, A.G. Orpen, I.D. Williams, Science 283 (1999) 1148.
[8] D.K. Kumar, A. Das, P. Dastidar, Cryst. Growth Des. 6 (2006) 1903.
[9] Y.F. Zhou, F.L. Jiang, D.Q. Yuan, Chem. Int. Ed. 43 (2004) 5665.
[10] S. Mukhopadhyay, W.H. Armstrong, J. Am. Chem. Soc. 125 (2003) 13010.
[11] X.M. Chen, G.F. Liu, Chem. Eur. J. 8 (2002) 4811.
[12] B.L. Chen, C.D. Liang, J. Yang, D.S. Contreras, Y.L. Clancy, E.B. Lobkovsky, O.M. Yaghi, S. Dai, Angew. Chem., Int. Ed. 45 (2006) 1390.
[13] H. Chun, D.N. Dybtsev, H. Kim, K. Kim, Chem. Eur. J. 11 (2005) 3521.
[14] D.F. Sun, R. Cao, Y.Q. Sun, W.H. Bi, D.Q. Yuan, Q. Shi, X. Li, Chem. Commun. (2003) 1528.
[15] Z.M. Sun, J.G. Mao, Y.Q. Sun, H.Y. Zeng, A. Clearfield, Inorg. Chem. 43 (2004) 336.
[16] F.N. Dai, H.Y. He, D.F. Sun, J. Am. Chem. Soc. 130 (2008) 14064.
[17] G.M. Sheldrick, SHELXS-97, Program for Crystal Structure Solution, Gottingen University, Germany, 1997.
[18] G.M. Sheldrick, SHELXL-97, Program for Crystal Structure Refinement, Gottingen University, Germany, 1997.
[19] J.-M. Lehn, Angew Chem., Int. Ed. 27 (1988) 89.
[20] C.Y. Su, A.M. Goforth, M.D. Smith, P.J. Pellechia, H.C. zur Loye, J. Am. Chem. Soc. 126 (2004) 3576.
[21] C.Y. Su, M.D. Smith, H.C. zur Loye, Angew. Chem., Int. Ed. 42 (2003) 4085.
[22] B. Zhao, P. Cheng, Y. Dai, C. Cheng, D.Z. Liao, S.P. Yan, Z.H. Jiang, G.L. Wang, Angew. Chem., Int. Ed. 42 (2003) 934.
[23] P.Q. Zheng, Y.P. Ren, L.S. Long, R.B. Huang, L.S. Zheng, Inorg. Chem. 44 (2005) 1190.
[24] L.M. Zheng, X. Fang, K.-H. Lii, H.-H. Song, X.-Q. Xin, H.-K. Fun, K. Chinnakali, I.A. Razak, J. Chem. Soc., Dalton Trans. (1999) 2311.
[25] M. Aoyagi, K. Biradha, M. Fujita, Bull. Chem. Soc. Jpn. 73 (2000) 1369.
[26] S. Noro, R. Kitaura, M. Kondo, S. Kitagawa, T. Ishii, H. Matsuzaka, M. Yamashita, J. Am. Chem. Soc. 124 (2002) 2568.
[27] S.D. Huang, R.-G. Xiong, Polyhedron 16 (1997) 3929.
[28] G.R. Desiraju, R.L. Harlow, J. Am. Chem. Soc. 111 (1989) 6757.
[29] G.S. Papaefstathiou, C. Milios, L.R. MacGillovray, Micropor. Mesopor. Mater. 71 (2004) 11.
[30] M.P. Suh, H.J. Choi, S.M. So, B.M. Kim, Inorg. Chem. 42 (2003) 676.
[31] Z.-Y. Fu, X.-T. Wu, J.-C. Dai, S.-M. Hu, W.-X. Du, H.-H. Zhang, R.-Q. Sun, Eur. J. Inorg. Chem. (2002) 2730.
[32] S.J.A. Pope, B.J. Coe, S. Faulkner, E.V. Bichenkova, X. Yu, K.T. Douglas, J. Am. Chem. Soc. 126 (2004) 9490.
[33] S.T. Wang, Y. Hou, E.B. Wang, Y.G. Li, L. Xu, J. Peng, S.X. Liu, C.W. Hu, New J. Chem. 27 (2003) 1144.
[34] M.P. Clares, J. Aguilar, R. Aucejo, C. Lodeiro, M.T. Albelda, F. Pina, J.C. Lima, A.J. Parola, J. Pina, J.S. De Melo, C. Soriano, E. García-España, Inorg. Chem. 43 (2004) 6114.